vol. 45, n.° 3, septiembre-diciembre de 2023
ISSN impreso: 0120-0283 • ISSN en línea: 2145-8553

General considerations on the genesis of Uranium and Vanadium occurrence in the Cretaceous sedimentary rocks of the Berlin Synclinal, Central Cordillera (Colombian Andes)

Andrés Cáceres-Bottia[1*]; Luis Carlos Mantilla-Figueroa[1]; Carlos Alberto Ríos-Reyes[1]; Robinson Pimiento-Rueda[1]

[1]Escuela de Geología, Universidad Industrial de Santander, Bucaramanga, Colombia. (*) acacerbo@correo.uis.edu.co; lcmantil@uis.edu.co; carios@uis.edu.co; robinsonpimientorueda@gmail.com

Abstract

The mineralization at the Berlin project in Colombia presents a huge interest based on its relatively high uranium and vanadium concentrations (0.11% U_3O_8) and (0.45% V_2O_5), with a suite of other economically interesting elements, all of them necessary to achieve the energy transition, including Y, Re, Ag, and P. The present research suggests a hypothesis for the U and V mineralization: an epigenetic origin. The results indicate that the source for U, V, and the other economic elements associated, were released from the black shales of the Abejorral Formation that is overlying a carbonate succession of Cretaceous wackestone. Those elements were transported in diagenetic fluids under specific physical and geochemical conditions. Efficient strata-bound trap occurred when the carbonate succession triggered a redox front that interacted not only with mineralized fluids, but organic matter and H_2S.

Keywords: Uranium; Vanadium; Epigenetic; Energy transition.

Consideraciones generales sobre la génesis de la ocurrencia de uranio y vanadio en las rocas sedimentarias Cretácicas del Sinclinal de Berlín Cordillera Central (Andes Colombianos)

Resumen

La mineralización en el proyecto Berlín en Colombia es de interés por varias razones, entre estas sus concentraciones relativamente altas de uranio (0,11% U_3O_8) y vanadio (0,45% V_2O_5), además de la aparición de otros elementos que pueden ser económicamente interesantes y necesarios para lograr la transición energética, tales como Y, Re, Ag y P. En el presente estudio se propone una hipótesis para el origen de la mineralización de uranio y vanadio: un origen epigenético. Los resultados indican que la fuente del uranio, el vanadio y los otros elementos económicos asociados proviene principalmente de las lutitas carbonosas de la formación Abejorral que sobreyacen una sucesión de *wackestones* del Cretácico. Los elementos de interés fueron transportados mediante fluidos diagenéticos bajo condiciones físicas y geoquímicas específicas. La trampa de la mineralización ocurre de manera estratoligada debido a un frente de reducción durante la interacción con materia orgánica y H_2S, la cual es detonada y atrapada por la sucesión de carbonatos.

Palabras clave: Uranio; Vanadio; Epigenético; Transición energética.

How to cite: Cáceres-Bottia, A.; Mantilla-Figueroa, L.C.; Ríos-Reyes, C.A.; Pimiento-Rueda. R. (2023). General considerations on the genesis of Uranium and Vanadium occurrence in the Cretaceous sedimentary rocks of the Berlin Synclinal, Central Cordillera (Colombian Andes). *Boletín de Geología, 45*(3), 79-93. https://doi.org/10.18273/revbol.v45n3-2023005

Introduction

The world is facing a huge environmental challenge created by greenhouse gas emissions. Global warming is a fact and decarbonization is a goal that must be accomplished in the medium-short term. Uranium and vanadium are two of the major players in the energy transition since uranium can produce energy from nuclear reactors with zero CO_2 emissions (IAEA, 2021) and vanadium is a primary component for batteries that can store energy generated by renewable sources (Kelley *et al*., 2017).

Uranium and vanadium are associated with different deposit models, but there are some examples where both are concentrated as principal commodities e.g., black shale (syngenetic and epigenetic), sandstone (epigenetic), and calcretes (supergene).

The increased demand for uranium and vanadium for energy transition has induced these types of deposits to reach higher levels of interest even though they are deemed as containing low grades in high tonnage.

Berlin project was classified as the typical syngenetic enrichment of black shale (Naranjo, 1983), however, Berlin project has shown an atypical enrichment of different metals by epigenetic processes, so the understanding of those processes could provide valuable tools for exploration.

Berlin project is located in the municipality of Samaná (Caldas Province), which is placed on the east flank of the Central Cordillera of Colombia (~100 km to the SE of the city of Medellin and ~140 km to the NW of the City of Bogotá) and correspond to an N-S elongated sedimentary sequence of a synclinal shape structure (INGEOMINAS, 1987). The presence of uranium mineralization in the cretaceous sedimentary rocks has been reported in several studies (INEA, 1981; IAEA, 1983; Naranjo, 1983; Garzón, 1984; González, 2001), with uranium concentrations ranging from 1000 and 2500 ppm of U_3O_8. This fact, together with the presence of other elements with economic potentials, such as V, Y, Re, Ag, and P, besides the relatively low contents of potentially problematic elements such as Se and As, make this sector of the Central Cordillera an area of great exploratory interest (Cáceres, 2012). For this reason, the company GaiaEnergy, a subsidiary of the Canadian company U3O8 Corp., developed in this area a drilling program between 2010 and 2011, to know and expand their potential uranium resources (www.u3o8corp.com). Despite the enormous economic attractiveness of these types of commodities, the project still lacks detailed geological studies that allow elucidation of the metallogenesis of uranium, vanadium, and other metals in the Colombian Andean orogenic system.

The increased demand for uranium and vanadium for energy transition has induced these types of deposits to reach higher levels of interest even though they are deemed as containing low grades in high tonnage. Many authors define these ranges, which are based on cut-off grade relationships; for example, Kyser and Cuney (2008) define the term 'low-grade' for deposits with grades of 0.1%. Currently, the Berlin low-grade deposit has a grade of 0.11% U_3O_8, compared to deposits such as unconformity-related ones that have grades of 5-19% U_3O_8.

In the above context, this study is focused on contributing to the knowledge of the uranium and vanadium metallogenesis in epigenetic systems, integrating geological and geodynamic context, mineralogical and petrographic characteristics of the mineralization and the host rock (paragenetic sequence), combined with the U-Pb age of mineralization.

Geological Setting

Berlin project is located in the Colombian Andean orogenic system (Figure 1), specifically in the Cajamarca-Valdivia terrane in the Central Continental Sub-plate realm (Cediel *et al*., 2003), or in the Tahami Terrain in the sense of Restrepo and Toussaint (2020). The Berlin project is located in the area of influence of the Palestine Fault system, which is associated with a crustal weakness zone ranging from 0.5 to 30 km wide (Page, 1986). Palestine fault is considered to have had a dextral displacement during the Neogene to Paleogene (Feininger, 1970).

The basement consists of metamorphic rocks of the Cajamarca Group, which has also been named Cajamarca Series (Nelson, 1962) or Complex (Maya and González, 1995), that is considered of Early Paleozoic age (Bürgl, 1966).

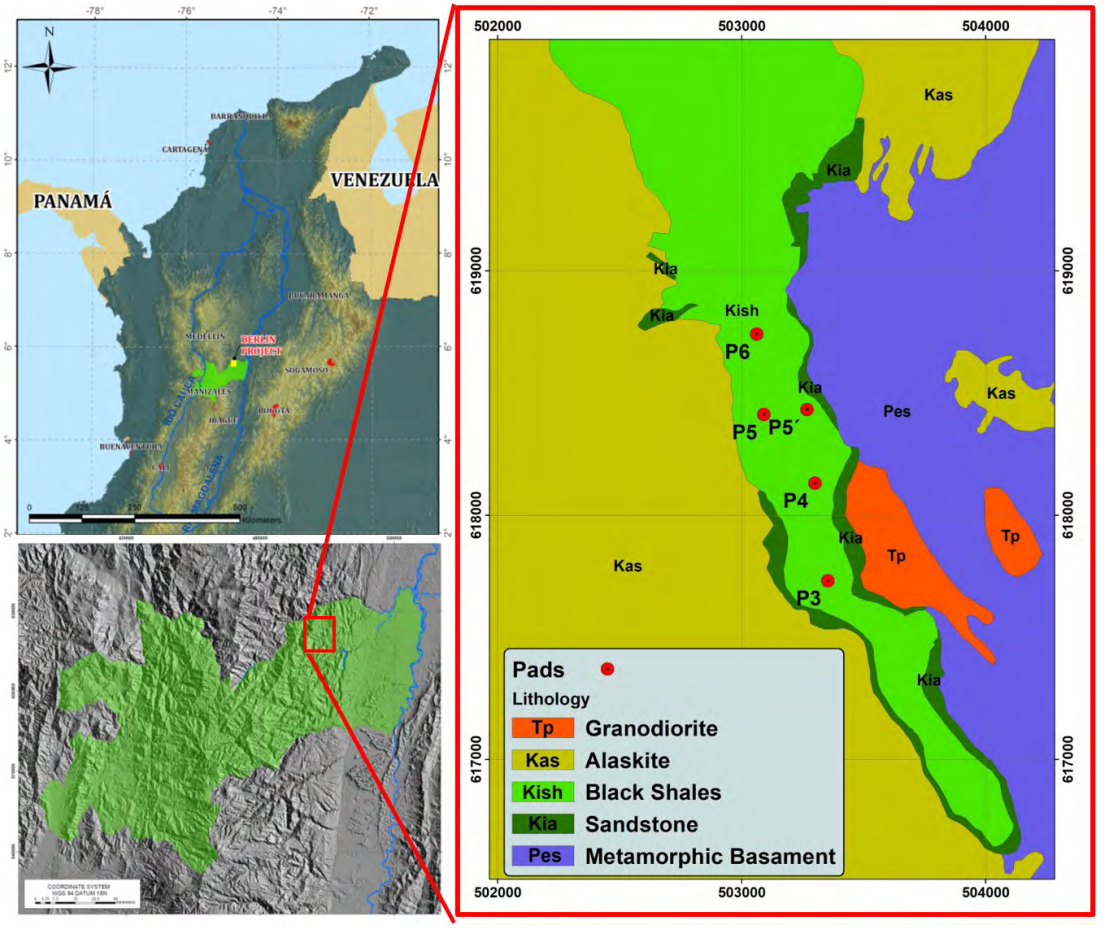

Figure 1. Left, location of the Berlin project in the Caldas Department. Right, a generalized geological map of the study area.

A sedimentary sequence that corresponds to a transitional continental-marine-lagoonal environment is found overlying discordantly the Cajamarca Group (Figure 2).

Four successions were recognized in the study area. Succession A: a terrigenous lithology (K1-Sj) of basal conglomerates interbedded with sandstones recorded the beginning of a back-arc extensional event at 150 Ma (Zapata *et al*., 2019). The clasts present within the conglomerate layers consist mainly of mafic and intermediate igneous fragments, metamorphic fragments, and milky white quartz. The upper part of this succession corresponds to a massive silicified, medium to coarse grain size, with poorly sorted and subangular grains of sandstone. The average thickness of the entire succession A is 36 m (Naranjo, 1983). Succession B: presents a gradation contact with succession A and corresponds to a fossiliferous calcareous mudstone, with the presence of well-preserved bivalves and gastropods (Figure 3A), deposited during basin deepening and the change to a marine environment that took place until Albian (100 Ma). The upper part of this succession is defined by a major erosional surface where the different grain size is easily observable between succession B and C (Figure 3B). This disconformity marked not just the change to a compressional tectonic event but the lower limit of the mineralization. Succession C: a muddy wackestone with the presence of reworked fossil fragments, displaying wavy lamination and a high content of authigenic apatite and bitumen (Figure 3C). This is consistent with either the increasing water energy or probably the relative shallowing of the basin (Edelman-Furstenberg, 2009; Zapata *et al*., 2019). This succession constitutes the mineralized level, which varies in thickness from 1 to 3.5 m, with a maximum thickness of 9.2 m (in a drillhole) and 6.7 m (in a trench). Succession D: the upper succession (b6-Be) corresponds to a deformed black carbonaceous shale with bioclast (Figure 3D), which may locally reach 600 m in thickness. This was deposited in a lagoonal environment and is related to the enclosing of the marine basin caused by the accretion of the Romeral terrane and the uplifting of the Cajamarca-Valdivia

terrain during Aptian to Albian (Cediel *et al*., 2003) or even Albian to Campanian (Zapata *et al*., 2019). All data were confirmed on fossil analysis, according to personal communication by Etayo-Serna, in Cáceres (2012).

A set of dikes and sills of andesitic to dacitic composition are found injecting the metamorphic and sedimentary rocks described above. Leucocratic (alaskites) and mesocratic (ranging from tonalite to granodiorite) plutons are recognized as the Samaná Igneous Complex, which is considered of Aptian-Albian age (119±10 Ma - K/Ar in hornblende) according to Barrero and Vesga (1976).

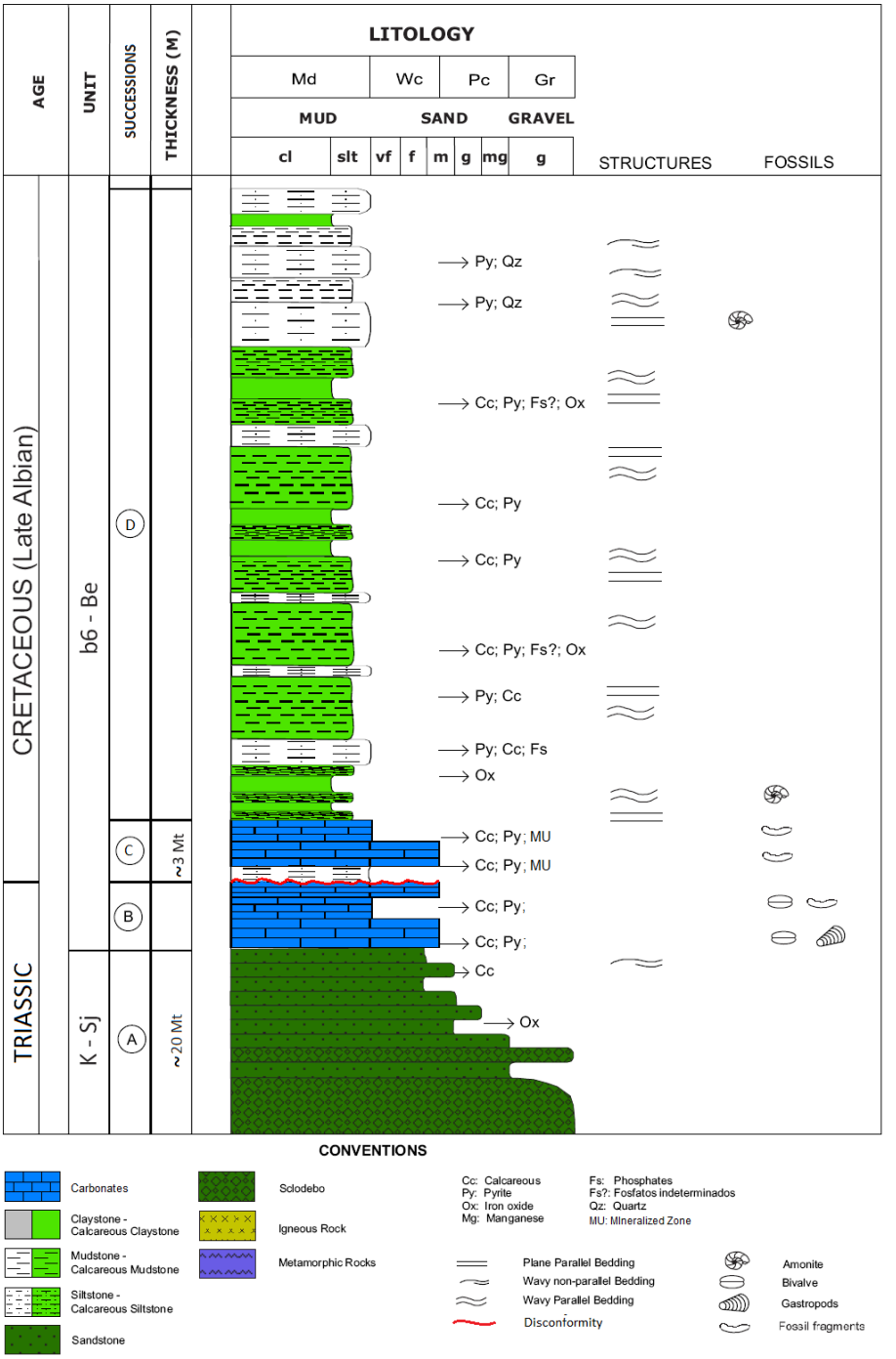

Figure 2. Stratigraphic column Berlin project and drill core description.

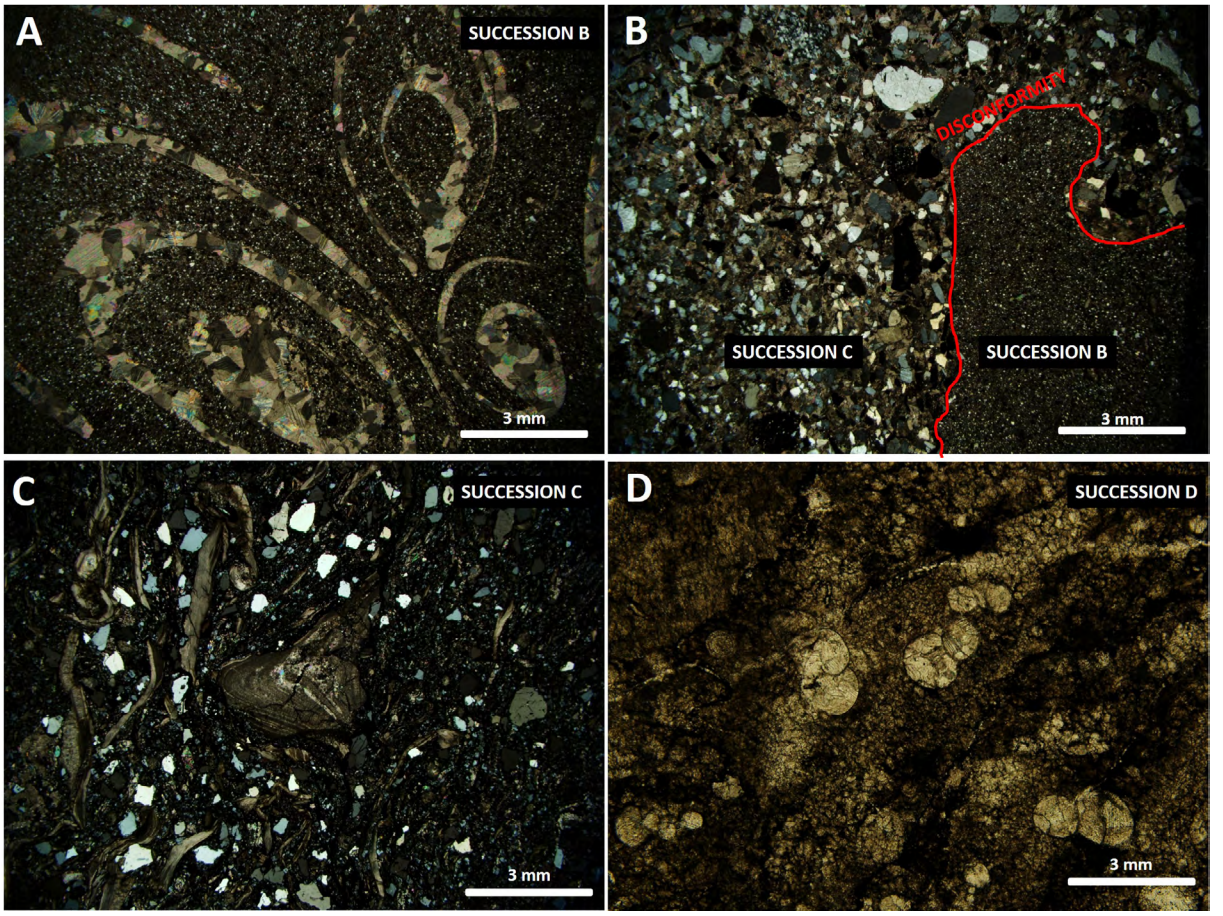

Figure 3. Cross-polarized transmitted light (A, B, and C). Plane-polarized transmitted light (D). **A.** Photomicrograph showing fossiliferous mudstone with bivalves and gastropods (succession B). **B.** Photomicrograph illustrating erosive surface (disconformity). Contact between successions B and C. **C.** Photomicrograph shows the muddy wackestone with reworked fossil fragments (succession C). **D.** Photomicrograph illustrating bioclast within succession D.

Sample Preparation and Analytical Methods

Six hundred fifty-six samples were taken from succession B, C, and D, during the drilling program of the U3O8 Corp during the resource estimation for the Berlin project (De Klerk *et al*., 2013). Nine polished thin sections of the succession C (mineralized layer) from boreholes DDB11, DDB16, DDB17, and DDB18 were used for petrographic analysis using reflected and transmitted light and scanning electron microscopy to establish the mineral assemblage. Sampling localities were selected considering a locality where the sequence is not inverted or intensively deformed (Figure 1, Table 1). Polished thin sections were also used for electron probe microanalysis (EPMA) with a JEOL JXA-8230 with five wavelength-dispersive spectrometers (WDS). EPMA using a JEOL JXA-8230 equipped with five wavelength-dispersive spectrometers (WDS). Acquisitions were obtained with a 15-kV accelerating voltage, 10-nA beam current, and 5 to 10 µm diameter defocused beam. Typical counting times were 10 s for major elements, 20 s for minor elements, and 30 to 40 s for trace elements.

Uraninites were dated by laser ablation using the polished thin section DDB13 by *in situ* U-Pb isotope ratios using a ThermoFinnigan Neptune high-resolution multicollector ICP-MS (HR-MC-ICP-MS), following the method of Chipley *et al*. (2007).

Isotopic compositions of carbon and oxygen were measured in the carbonates of the borehole DDB16 using a Finnigan MAT 252 isotope ratio mass spectrometer (IRMS). $\delta^{13}C$ results are relative to the PDB standard, while $\delta^{18}O$ results are relative to the Vienna Standard Mean Ocean Water (V-SMOW). All analyzes were conducted at Queen's Facility for Isotope Research Lab.

Table 1. Location of the samples used in this paper. Coordinate system: UTM 18N.

Borehole	Pad	Depth	Azimut	Dip	Easting	Northing	Altitude
DDB11	P4	166	268	65	503298	618115	705
DDB13	P5	350	69	61	503267	618432	730
DDB16	P5	223	252	52	503117	618436	688
DDB17	P6	287	238	85	503065	618733	681
DDB18	P6	250	245	45	503064	618732	681

Results

Paragenetic sequence

The paragenetic sequence recognized in the lithology that constitutes the mineralized level (succession C) is depicted in Table 2, emphasizing the diagenetic process.

Quartz and muscovite conform to the detrital minerals that remained in the samples. Calcite Sage 1 occurs as fossil replacement and as cement formed during burial.

Petrographic analysis reveals textural and structural features and the mineral composition within the rocks that contain the mineralization. The occurrence of detrital quartz provides the primary porosity that allows diagenetic fluids to percolate and precipitate calcite (stage 2), authigenic apatite, and bitumen (Figure 4A). Also, many samples revealed intense fracturing of the clastic quartz, which can be associated with tectonic efforts caused by the inversion of the extensional regime during the collision of the oceanic lithosphere which started in the late Mesozoic (Cediel *et al*., 2003). Detrital muscovite is observed with alteration to the edge (Figure 4B).

Table 2. Generalized paragenesis for the Berlin project.

Minerals	Detrital minerals	Diagenesis	
		Early	Late
Quartz	----------		
Moscovite	------		
Calcite Stage 1		----------	
Apatite		----------	
V-Ba rich mica (chernykhite)		------	
Bitumen		----------	
Uraninite		----------	
Pyrite		----------	
Sphalerite		------	
Calcite Stage 2			--------
As-Ni-S Minerals			-------
Calcite Vainlets			-----

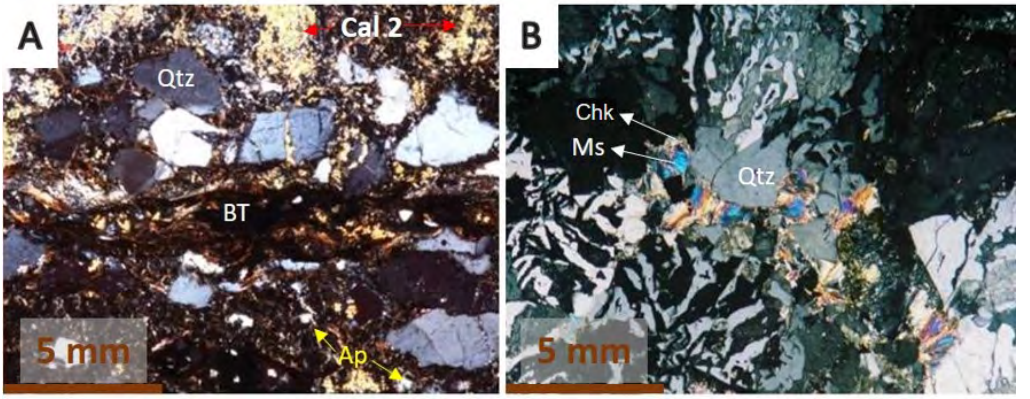

Figure 4. Photomicrographs of the textural microstructural features Berlin project. **A.** Fracture quartz grains in an interstitial matrix with calcite (stage 2), apatite, and bitumen. **B.** Detrital muscovite with alteration to the edge. Quartz (Qtz), Calcite Stage 2 (Cal 2), Apatite (Ap), Bitumen (BT), Muscovite (Ms) and Chernykhite (Chk) (adapted and modified after Pimiento, 2011).

Electron microprobe and SEM disclose the diagenesis process in detail. Authigenic apatite (Figure 5A) and bitumen (Figures 5B, 5E, and 5F), were incorporated into the mineralized layer, along with uraninite and chernykhite (Ba-V-rich mica). Electron probe microanalysis allowed identifying the replacement of muscovite by chernykhite (Figures 5C and 5D). Bitumen is observed filling pore spaces between the apatite (Figure 5E) and calcite stage 2 (Figure 5F). Authigenic apatite is zoned (Figure 5G), showing an increase in Y and U from core to rim. Pyrite, Sphalerite (Figure 5H), and other sulfides, as well as bitumen (Figure 5H), fill the spaces formed between the apatite, calcite stage 2, and detrital quartz. Late diagenesis (3) is characterized by the presence of Ni-As sulfides, which replace sphalerite (Figure 5I), and a second generation of calcite, which occurs as grooves and veinlets that cross-cut apatite and bitumen. The formation of this calcite can be attributed to the dissolution and re-precipitation processes of carbonate.

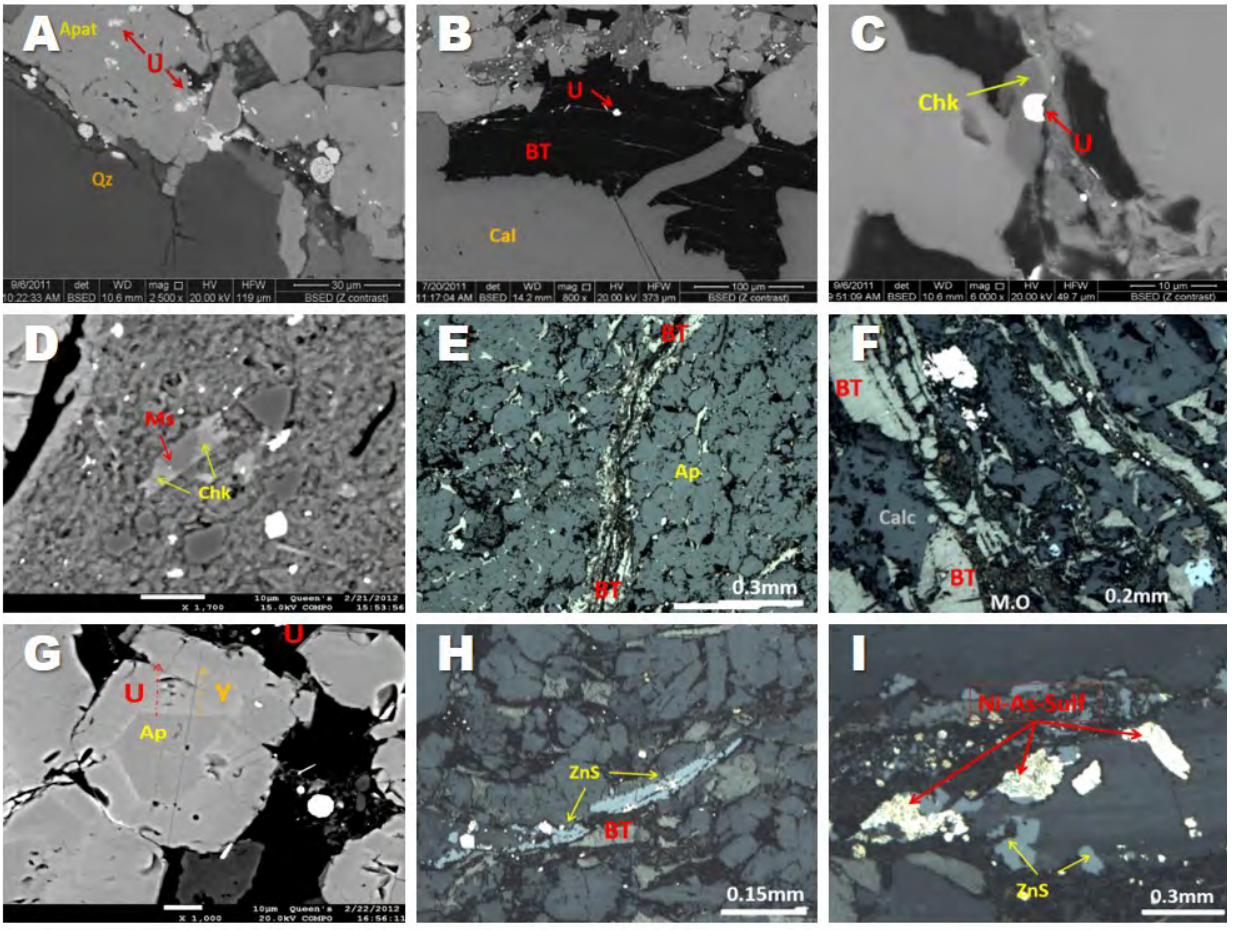

Figure 5. A. Back-scattered electron image of textural relationships between uraninite and apatite. **B.** Back-scattered electron image of uraninite within bitumen being cross-cut by calcite. **C.** Back-scattered electron image of uraninite and chernykhite. **D.** Back-scattered electron image of muscovite replaced by chernykhite. **E.** Plane-polarized reflected light image of bitumen filling spaces between the apatite. **F.** Plane-polarized reflected light image of bitumen and organic matter filling spaces between calcites. **G.** Back-scattered electron image of apatite uranium-yttrium zonation. **H.** Plane-polarized reflected light image of sphalerite following the pattern of bitumen. **I.** Sphalerite was replaced by Ni-As sulfides. U: Uraninite; Ap: Apatite; BT: Bitumen; M.O: Organic matter; Cal: Calcite; Chk: Chernykhite; Ms: Muscovite; ZnS: Sphalerite.

Mineral Chemistry

Uraninite grains were analyzed by electron microprobe analysis and scanning electron microscopy (Figure 6). Uraninite contains up to 90 wt% U and other elements, such as rare earth elements (REE), Ca, and radiogenic Pb (Alexandre and Kyser, 2005). Electron back-scatter images show that the average size for uraninite is less than 10 µm, so some results obtained using electron microprobe analysis reveal "contamination" from surrounding material due to the small size of uraninite, which will complicate isotopic dating. The chemical composition of uraninite is quite variable, with UO_2 from 81.47 to 94.44 wt% (Table 3).

Chemical compositions of the uraninite indicate negative correlations between UO_2 and SiO_2, V_2O_3, Cr_2O_3, MnO, P_2O_5, and FeO, and positive correlations between UO_2 and ThO_2 and PbO (Figure 7).

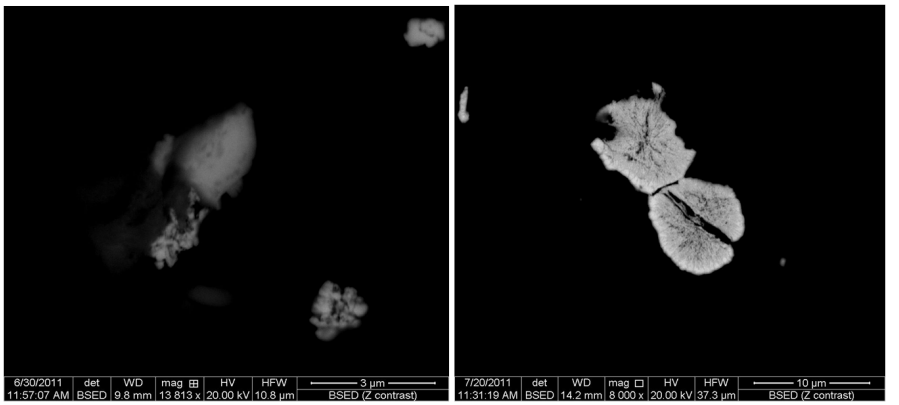

Figure 6. Back-scattered electron images of uraninite grains.

Table 3. Electron microprobe analysis and calculated U-Pb ages for uraninite from the Berlin project. Chemical composition is expressed in wt%.

	SiO_2	TiO_2	V_2O_3	Cr_2O_3	MnO	P_2O_5	FeO	UO_2	MgO	ThO_2	PbO	Y_2O_3	CaO	Total
11 uran 1	0.90	0.60	0.55	0.03	0.06	0.16	0.50	86.94	0.01	0.02	0.17	0.91	3.60	94.46
11 uran 2	1.08	0.69	1.09	0.05	0.07	1.13	0.54	80.21	0.00	0.00	0.00	0.74	4.42	90.07
11 uran 3	0.35	0.57	0.26	0.01	0.00	0.07	0.15	92.44	0.00	0.07	0.71	0.92	2.25	97.82
18 uran 1	0.62	0.58	0.43	0.05	0.10	0.39	0.68	88.17	0.02	0.02	0.13	0.72	2.76	94.84
18 uran 2	0.54	0.64	0.55	0.07	0.07	1.20	0.35	84.88	0.02	0.02	0.19	0.68	3.47	92.75
18 uran 3	0.86	0.66	0.68	0.10	0.09	1.01	0.53	81.47	0.02	0.00	0.11	0.67	2.43	88.84
16 uran 1	0.45	1.19	0.19	0.01	0.00	0.20	0.06	88.93	0.00	0.08	0.70	0.57	2.65	95.09
median	0.62	0.64	0.55	0.05	0.07	0.39	0.50	86.94	0.01	0.02	0.17	0.72	2.76	94.46
mean	0.69	0.70	0.53	0.05	0.05	0.59	0.40	86.15	0.01	0.03	0.29	0.75	3.08	93.41

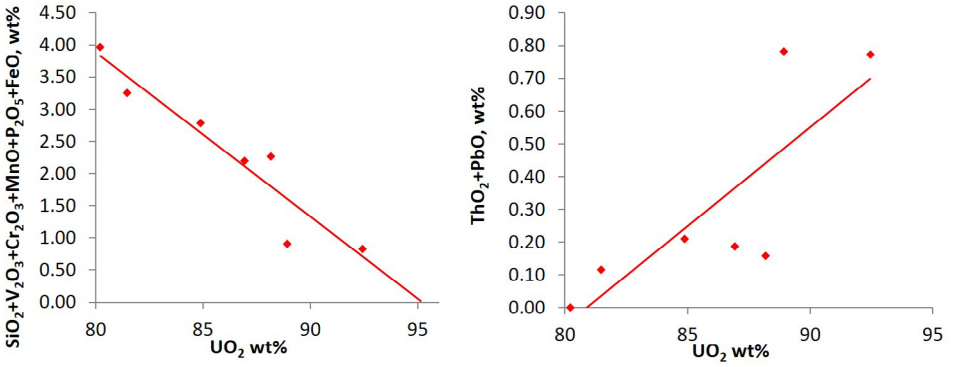

Figure 7. Correlations between UO_2 and other oxides (adapted and modified after Cáceres, 2012).

These correlations that the oxides that positively vary with UO_2 correspond to the original mineralogy of the uraninite present, whereas those that are negatively correlated correspond to contamination, which would occur if uraninite particles were small enough (<10 µm) so that the microprobe beam diameter (5 µm) encompassed surrounding elements of other material as well as the uraninite. Uraninite may incorporate Th, Ca, REE, and Y during its initial formation, and Pb is added later through decay. It is assumed that the uraninite does not initially contain Si, Fe, P, Mn, Cr, and V, but rather that these elements were introduced by contamination of the microprobe beam. Results of microprobe analysis reveal that the concentration of contaminants is negatively correlated with UO_2 so pure uraninite is when contaminant concentration is zero. By extrapolating the concentration of contaminants to zero, we calculated the best estimation for uraninite composition (Figure 8).

The estimated age of the Berlin project is 67±15 Ma. This age calculation is based on the extrapolated chemical composition of uraninite, and the assumption that all Pb contained in the analysis of the uraninite is radiogenic (Bowles, 1990). Pb coming from Th is negligible, as Th contents are low. The amount of ^{206}Pb (atom %wt) was calculated from the PbO content, and the amount of ^{238}U (atom %wt) was calculated from the total UO_2 content, as determined from the microprobe analysis best-estimated values of uraninite (UO_2 = 94.3 wt%; U = 94.3*1.134¥ = 83.16, and PbO = 0.8 wt%; Pb = 0.8* 0.928§ = 0.76). Age calculations were carried out using the empirical formula of Ranchin (1968), which is the best approach for ages less than 200 Ma (Alexandre and Kyser, 2005).

Age estimates based on correlations

The age of formation of the uraninite in the Berlin project can also be deciphered by extrapolating the chemical U-Pb ages to the time when the content of the contaminating elements is zero; the inferred age of 75±15 Ma, estimated from the intercept of the total contaminant elements (Figure 9), is similar to the age of 67 Ma obtained by the best-estimated U-Pb values from the uraninite.

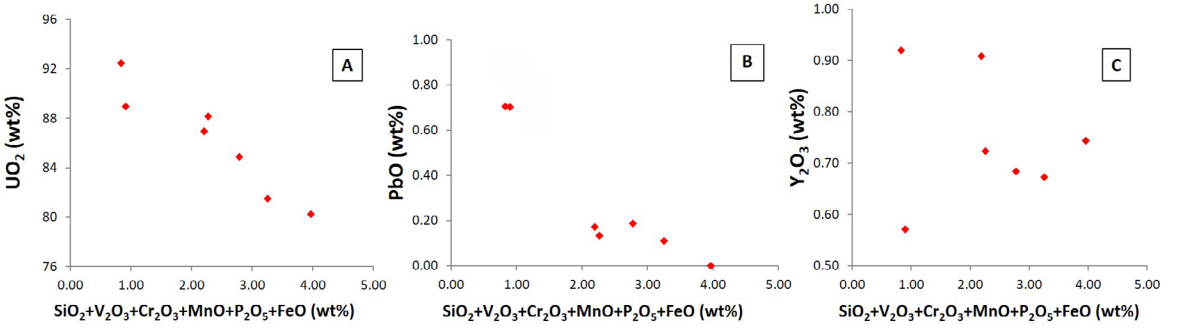

Figure 8. Negative correlations between oxides introduced by contamination (SiO_2, V_2O_3, Cr_2O_3, MnO, P_2O_5, and FeO) and some oxides initially in uraninite: **A.** UO_2, **B.** PbO and **C.** Y_2O_3 (adapted and modified after Cáceres, 2012).

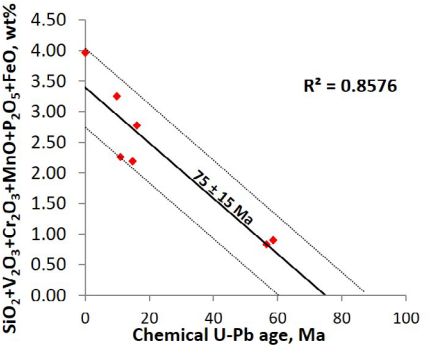

Figure 9. Combined concentration of contaminating uraninite elements (SiO_2, V_2O_3, Cr_2O_3, MnO, P_2O_5, and FeO contents) as a function of the estimated chemical U-Pb age (adapted and modified after Cáceres, 2012).

U/Pb geochronology

U-Pb dating on uraninites was performed on one polished thin section by laser ablation-inductively coupled plasma-mass spectrometry (LA-ICP-MS). According to Cáceres (2012), uranium mineralization occurred at 53±11 Ma based on $^{204}Pb/^{238}U$ data obtained by laser ablation of two uraninites (Figures 10 and 11), which coincides with the calculated chemical U/Pb ages (67±15 Ma).

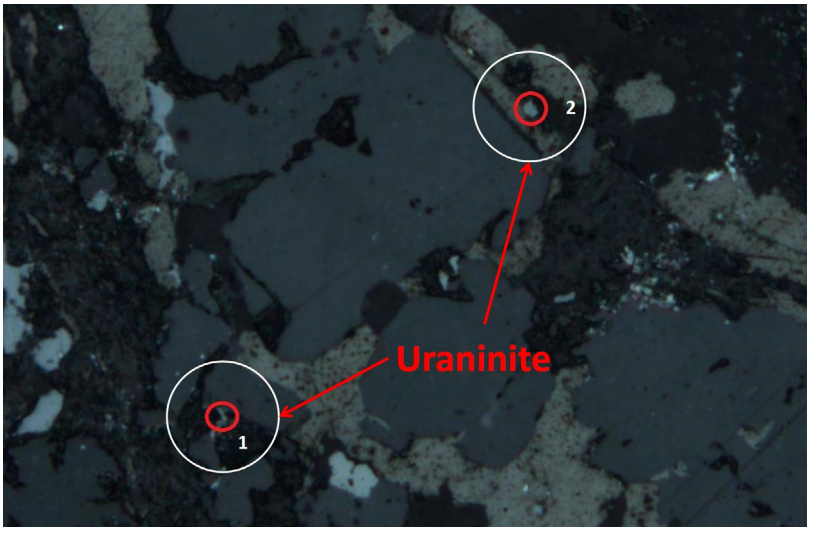

Figure 10. Plane-polarized reflected light image showing uraninite chosen for ablation.

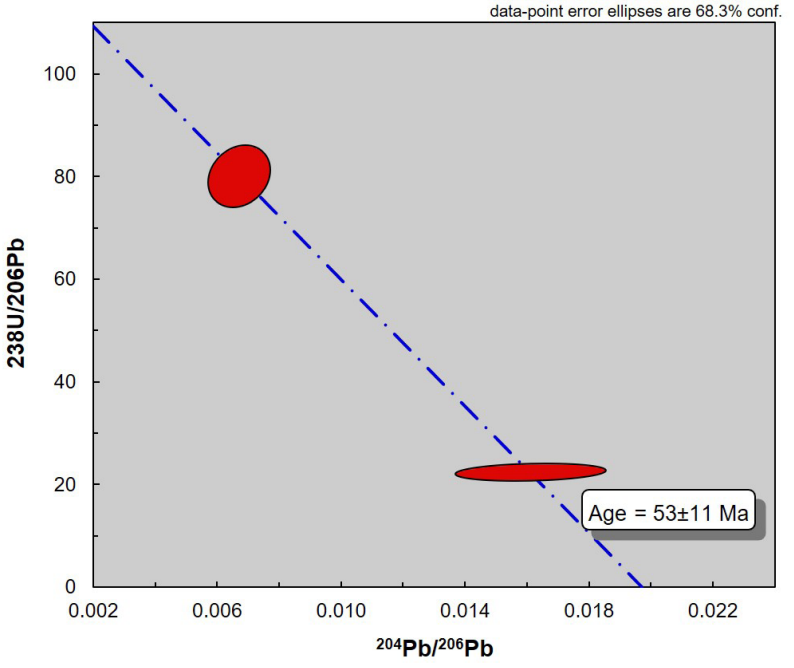

Figure 11. U-Pb inverse Concordia diagram from isotopic analysis by LA-ICPM-MS of uraninites from Berlin project.

Stable Isotopes

Calcite from fossils and the matrix were sampled from a mineralized section of drill core DDB16. Around 3 mg were taken using a scalpel under a binocular microscope. The matrix calcite crystals were very small (<0.5 mm); therefore, it is possible that samples contained some contamination from the surrounding diagenetic apatite and organic matter. Calcite samples were dissolved in 100% phosphoric acid at 25°C, and the CO_2 gas released was analyzed in an isotope ratio mass spectrometer for carbon and oxygen isotopic compositions. The values obtained are reported in units per mil (‰). Calcite within the fossils showed $\delta^{13}C$ and $\delta^{18}O$ values of -0.4 and +22.7, respectively, whereas calcite in the matrix, showed the following values: $\delta^{13}C$ = -1.8 and $\delta^{18}O$ = +18.1 (Figure 12). These stable isotopic data for calcite within the fossils correspond to calcite formed between 10 and 25°C in a marine environment, whereas those values of calcite in the matrix correspond to calcite formed at 40°C in a fresh-water environment (Keith and Weber, 1964; Kim and O'Neil, 1997) during diagenesis. The high $\delta^{13}C$ value of calcite in the matrix also indicates a minimal contribution from organic matter.

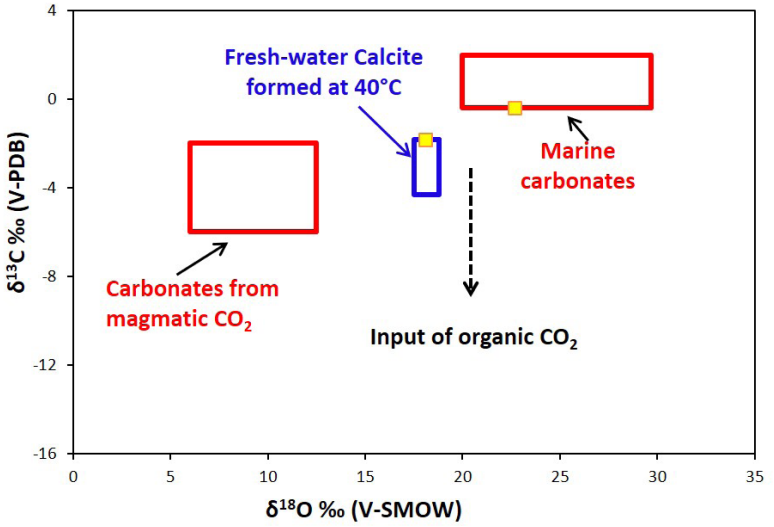

Figure 12. Carbon and oxygen isotopic compositions of calcite from fossils and calcite from the matrix in the mineralized sample from drill hole DDB16. Samples are represented by yellow squares. The field for carbonates from magmatic CO_2 is from Des Marais and Moore (1984) and the field for marine carbonates at different temperatures is from Kim and O'Neil (1997).

Discussion

In order to understand the mineralization observed at the Berlin project is necessary to state a geodynamic context whereby the diagenetic fluids triggered the remobilization, transported, and trapped the elements involved during the enrichment process. The Mesozoic basin where the sedimentary sequence was deposited (successions A, B, C, and D) underwent two mains regional upliftings. The first, a minor uplift registered in the unconformity (erosion level) between successions B and C as a response to dextral accretion of Romeral terrain during Albian (Cediel *et al.,* 2003; Vinasco, 2019; Cediel, 2019; Zapata *et al*., 2019), the second and most important, the collision of the Farallon Plate and accretion of the Dagua terrane during Paleocene-Lower Eocene (Cediel *et al.,* 2003; Ramos, 2009) that triggered the major charge of diagenetic fluids flowing registered by uranium precipitation (53±11 and 67±15 Ma).

Geochemical analysis conducted in 656 samples collected from drill cores revealed a straight correlation between U and V concentration on each succession.

The results suggest that succession D is the source of the metals. The average concentration of U and V in shales is 4 ppm U and 130 ppm V (Shiller and Boyle, 1987; Kyser and Cuney, 2008). The background of these elements in succession D is higher than normal, containing about 58 ppm U and 1380 ppm V respectively. Rock eval analyses showed a correlation between the depletion of organic fraction and different elements in the lower section of this succession (Cáceres, 2012), which suggests remobilization during diagenesis.

In the succession C is located the strata-bound mineralization. Textural and chemical composition make this succession the optimal trap. Grain size (good primary porosity) and carbonate composition interacted with diagenetic fluids generating the conditions for uranium and vanadium to precipitate. Uranium and vanadium content decreased drastically in the fossiliferous mudstone (succession B), which acted as an impermeable boundary for diagenetic fluids, confirming that the unconformity level between succession B and C is the lower limit of the mineralization. Geochemical conditions of the fluids involved in the diagenesis also play a major role in the remobilization of the elements.

In epigenetic environments, such as uranium sandstone deposits, U and V thermodynamic conditions where these two elements are presented have been well studied (Wanty and Goldhaber, 1992; Spirakis, 1996; Kyser and Cuney, 2008) and state important parameters.

To remobilize a large amount of uranium from the black shale (succession D) at that temperature mentioned, geochemical fluid characteristics had to be oxidized, alkaline, and carbonate-rich coupled with humic acids released during diagenesis of the black shales and also with strong anions such as F^-, Cl^-, CO_3^{2-} and PO_4^{3-} which increase U and V solubility (Kinney and Schwartz, 1957; Langmuir, 1978; Wanty *et al*., 1990; Galindo *et al*., 2007; Kyser and Cuney, 2008). Fluoride and phosphate complexes can transport a significant amount of uranium (Kyser and Cuney 2008), while vanadium is mainly transported by organic complexes (Spirakis, 1996) and fluoride complexes (Wanty *et al*., 1990). Elements such as Zn are transported by chloride complexes.

Paragenetic sequence confirmed the presence of each of the anions above mentioned with the occurrence of authigenic apatite ($Ca_5(PO_4)_3$ (F, Cl, $OH)_2$). Euhedral diagenetic apatite grains exhibit authigenic overgrowth and compositional variation from the core, with an increase of uranium and yttrium toward the rim (Figure 6G).

Crystallization of authigenic apatite in a carbonate succession during diagenesis could be represented by the following equation:

$$5CaCO_3 + 3PO_4^{-3} + F^- \rightleftharpoons Ca_5(PO_4)_3F + 5CO_3^{-2}$$

When authigenic apatite seized anions that provided U and V solubility, hydrogen sulfide coupled with organic complexes worked as reductant agents, triggering uraninite and chernykhite mineralization at the Berlin project. Textural and chemical relationships indicate that uraninite precipitated almost at the same time as apatite.

The presence of H_2S is documented by the occurrence of cogenetic sulfurs such as sphalerite and pyrite.

Detrital muscovite had a relevant role during the entry of diagenetic fluids by trapping and integrating V^{+3} in its mineral structure by replacing Al^{+3} during the redox process. Microprobe investigation showed that chernykhite, a vanadium-rich mica, was formed by alteration and replacement in the edges of the muscovite (Figure 6D).

In a redox environment, the vanadium is incorporated into pre-existing micas or clays. Vanadium may replace Al^{+3} by isomorphic substitution in muscovite based on similar characteristics of ionic radius and electronegativity (Cai *et al*., 2015; Zheng *et al*., 2017). Organic complexes such as humic acids play an important role by increasing aluminum solubility (remobilizing it from clays) and simultaneously work as a reductant agent for vanadium (Spirakis, 1996).

Carbonates that were released during apatite crystallization combined with Ca anions precipitated calcite stage 2. Diagenetic fluids changed to a more reduced condition, allowing Ni and As to replace Zn in the sphalerite.

Conclusions

Geodynamic events that occurred at Central Cordillera are correlated with the diagenetic peak reported by uraninite dating.

For uraninites, the chemical U-Pb age calculated using microprobe analysis was 67±15 Ma and the U-Pb isotopic age is 53±11 Ma.

Uranium and vanadium strata-bound mineralization at the Berlin project corresponds to an epigenetic event that occurred in a muddy wackestone with the presence of reworked fossil fragments.

The black shale of the Abejorral Formation was the source of uranium and vanadium, which were remobilized by diagenetic processes.

Geochemical characteristics of the diagenetic fluids had to be oxidized, alkaline, and carbonate-rich coupled with humic acids with strong anions such as F^-, Cl^-, CO_3^{2-} and PO_4^{3-} at temperatures below 200°C, to be effective for the transport of the elements of interest.

Succession C acted as an efficient chemical trap that allowed authigenic apatite, uraninite, sphalerite, and chernykhite to precipitate with the aid of reductant agents such as H_2S and other organic complexes.

Acknowledgments

My gratitude to Kurt Kyser who guided me in this research. My gratitude also to the Queen's Facility for Isotope Research lab staff, specifically April Vuletich, Alan Grant, Don Chipley, Evelyn Leduc, and Brian Joy, who guided me in each step of the Lab. The authors would like to thank U3O8 Corp which funded this work and provided all the samples for this study.

References

Alexandre, P.; Kyser, K. (2005). Effects of cationic substitutions and alteration in uraninite, and implications for the dating of uranium deposits. *The Canadian Mineralogist*, *43*(3), 1005-1017. https://doi.org/10.2113/gscanmin.43.3.1005

Barrero, D.; Vesga, C. (1976). Geología de la Plancha 188 - La Dorada, Esc 1:100000. Instituto Colombiano de Geología y Minería (INGEOMINAS).

Bowles, J. (1990). Age dating of individual grains of uraninite in rocks from electron microprobe analyses. *Chemical Geology*, *83*(1-2), 47-53. https://doi.org/10.1016/0009-2541(90)90139-X

Bürgl, H. (1966). The orogenesis in the Andean system of Colombia. *Tectonophysics*, *4*(4-6), 429-443. https://doi.org/10.1016/0040-1951(67)90009-1

Cáceres, A. (2012). Genesis of the sediment-hosted uraniferous phosphate deposit in the Berlin Project, Central Cordillera, Colombia, and its implications for exploration. MSc Thesis. Queen´s University, Canada.

Cai, Z.L.; Zhang, Y.M.; Liu, T.; Huang, J. (2015). Vanadium extraction from refractory stone coal using novel composite additive. *Jom*, *67*(11), 2629-2634. https://doi.org/10.1007/s11837-015-1611-5

Cediel, F. (2019). Phanerozoic Orogens of Northwestern South America: Cordilleran-Type Orogens. Taphrogenic Tectonics. The Maracaibo Orogenic Float. The Chocó-Panamá Indenter. In: F. Cediel, R.P. Shaw (eds.). *Geology and Tectonics of Northwestern South America* (pp. 3-95). Frontiers in Earth Sciences. Springer. https://doi.org/10.1007/978-3-319-76132-9_1

Cediel, F.; Shaw, R.P.; Cáceres, C. (2003). Tectonic assembly of the Northern Andean block. In: C. Bartolini, R.T. Buffler, J. Blickwedw (eds.). *The Circum-Gulf of Mexico and Caribbean: Hydrocarbon habitats, basin formation, and plate tectonics* (pp. 815-848). American Association of Petroleum Geologists. https://doi.org/10.1306/M79877C37

Chipley, D.; Polito, P.A.; Kyser, T.K. (2007). Measurement of U-Pb ages of uraninite and davidite by laser ablation-HR-ICP-MS. *American Mineralogist, 92*(11-12), 1925-1935. https://doi.org/10.2138/am.2007.2226

de Klerk, L.; Niemann, P.; Miller, P.; Véliz, P.; Corley, D. (2013). Preliminary economic assessment on the Berlin deposit-Colombia. Australia, Tenova Mining & Minerals (Australia) Pty Ltd.

Des Marais, D.J.; Moore, J.G. (1984). Carbon and its isotopes in mid-oceanic basaltic glasses. *Earth Planetary Sciences Letter*, *69*(1), 43-57. https://doi.org/10.1016/0012-821X(84)90073-6

Edelman-Furstenberg, Y. (2009). Cyclic upwelling facies along the Late Cretaceous southern Tethys (Israel): taphonomic and ichnofacies evidence of a high-productivity mosaic. *Cretaceous Research*, *30*(4), 847-863. https://doi.org/10.1016/j.cretres.2009.01.005

Feininger, T. (1970). The Palestina Fault, Colombia. United States Department of the Interior Geological Survey.

Galindo, C.; Mougin, L.; Fakhi, S.; Nourreddine, A.; Lamghari, A.; Hannache, H. (2007). Distribution

of naturally occurring radionuclides (U, Th) in Timahdit black shale (Morocco). *Journal of Environmental Radioactivity*, *92*(1), 41-54. https://doi.org/10.1016/j.jenvrad.2006.09.005

Garzón, T. (1984). Síntesis de los trabajos geológicos - mineros realizados en el prospecto Urano-Fosfático de Berlín-Caldas. Instituto de Asuntos Nucleares (IAN).

González, H. (2001). Memoria explicativa. Mapa Geológico del Departamento de Antioquia. Geología, recursos minerales y amenazas potenciales, INGEOMINAS.

IAEA (1983). Prospección de Uranio, Colombia. Conclusiones y recomendaciones. IAEA/UNDP-COL-76-031-TR Terminal Report. International Atomic Energy Agency.

IAEA (2021). Releases Report on Nuclear Energy for a Net Zero World Ahead of COP26 Climate Summit. International Atomic Energy Agency.

INEA (1981). Columna estratigráfica generalizada Berlín (Caldas) Antioquia - Uranio en rocas fosfóricas del Dpto. de Boyacá. Instituto de Ciencias Nucleares y Energías Alternativas.

INGEOMINAS (1987). Recursos Minerales de Colombia. Publicaciones especiales del INGEOMINAS, Bogotá, D.C.

Keith, M.L.; Weber, J.N. (1964). Carbon and oxygen isotopic composition of selected limestones and fossils. *Geochimica et Cosmochimica Acta*, *28*(10-11), 1787-1816. https://doi.org/10.1016/0016-7037(64)90022-5

Kelley, K.D.; Scott, C.; Polyak, D.E.; Kimball, B.E. (2017). Vanadium (No. 1802-U). US Geological Survey. https://doi.org/10.3133/pp1802U

Kim, S.; O'Neil, J. (1997). Equilibrium and nonequilibrium oxygen isotope effects in synthetic carbonates. *Geochimica et Cosmochimica Acta*, *61*(16), 3461-3475. https://doi.org/10.1016/S0016-7037(97)00169-5

Kinney, C.R.; Schwartz, D. (1957). Partial air oxidation of Chattanooga uraniferous black shale. *Industrial and Engineering Chemistry*, *49*(7), 1125-1130. https://doi.org/10.1021/ie50571a036

Kyser, K.; Cuney, M. (2008). Recent and not-so-recent development in uranium deposits and implication for exploration. Mineralogical Association of Canada Short Course Series Vol. 39. Quebec. 221-240.

Langmuir, D. (1978). Uranium solution-mineral equilibria at low temperatures with applications to sedimentary ore deposits. *Geochimica et Cosmochimica Acta*, *42*(6), 547-569. https://doi.org/10.1016/0016-7037(78)90001-7

Maya, M.; González H. (1995). Unidades litodémicas en la Cordillera Central de Colombia. *Boletín Geológico*, *35*(2-3), 43-57. https://doi.org/10.32685/0120-1425/bolgeol35.2-3.1995.316

Naranjo, J.L. (1983). Investigación del potencial uranífero en los shales negros del sinclinal de Berlín, Departamento de Caldas. Undergraduate Thesis. Universidad Nacional de Colombia.

Nelson, H.W. (1962). Contribución al conocimiento de la Cordillera Central de Colombia sección entre Ibagué y Armenia. *Boletín Geológico, 10*(1-3), 161-202. https://doi.org/10.32685/0120-1425/bolgeol10.1-3.1962.302

Page, W.D. (1986). Geología sísmica y sismicidad del noroeste de Colombia, Medellín, Woodward-Clyde Consultants, ISA, Integral, p. 1-156.

Pimiento, R. (2011). Mineralogía y petrografía de la mineralización de uranio en fosforitas del cretácico inferior, sinclinal de Berlín, Cordillera Central (departamento de Caldas, Colombia). Undergraduate Thesis. Universidad Industrial de Santander.

Ramos, V.A. (2009). Anatomy and global context of the Andes: Main geologic features and the Andean orogenic cycle. In: S.M. Kay, V.A. Ramos, W.R. Dickinson (eds.). *Backbone of the Americas: Shallow Subduction, Plateau Uplift, and Ridge and Terrane Collision* (pp. 31-65). vol. 204. The Geological Society of America. https://doi.org/10.1130/2009.1204(02)

Ranchin, G. (1968). Contribution à l'étude de la répartition de l'uranium à l'état de traces dans les roches granitiques saines: les uraninites à teneur élevée du Massif de Saint-Sylvestre (Limousin, Massif Central français). *Sciences dela Terre*, *13*, 159-198.

Restrepo, J.J.; Toussaint, J.F. (2020). Tectonostratigraphic terranes in Colombia: An update. First part: Continental terranes. In: J. Gómez, D. Mateus-Zabala (eds.). *The Geology of Colombia* (pp. 37-63). Volume 1, chapter 3. Servicio Geológico Colombiano. https://doi.org/10.32685/pub.esp.35.2019.03

Shiller, A.M.; Boyle, E.A. (1987). Dissolved vanadium in rivers and estuaries. *Earth and Planetary Science Letters*, *86*(2-4), 214-224. https://doi.org/10.1016/0012-821X(87)90222-6

Spirakis, C.S. (1996). The roles of organic matter in the formation of uranium deposits in sedimentary rocks. *Ore Geology Reviews*, *11*(1-3), 53-69. https://doi.org/10.1016/0169-1368(95)00015-1

Vinasco, C. (2019). The romeral shear zone. In: *Geology and Tectonics of Northwestern South America* (pp. 833-876). Springer, Cham. https://doi.org/10.1007/978-3-319-76132-9_12

Wanty, R.B.; Goldhaber, M.B.; Northrop, H.R. (1990). Geochemistry of vanadium in an epigenetic, sandstone-hosted vanadium-uranium deposit, Henry Basin, Utah. *Economic Geology, 85*(2), 270-284. https://doi.org/10.2113/gsecongeo.85.2.270

Wanty, R.B.; Goldhaber, M.B. (1992). Thermodynamics and kinetics of reactions involving vanadium in natural systems: Accumulation of vanadium in sedimentary rocks. *Geochimica et Cosmochimica Acta*, *56*(4), 1471-1483. https://doi.org/10.1016/0016-7037(92)90217-7

Zapata, S.; Cardona, A.; Jaramillo, J.S.; Patiño, A.; Valencia, V.; León, S.; Mejía, D.; Pardo-Trujillo, A.; Castañeda, J.P. (2019). Cretaceous extensional and compressional tectonics in the Northwestern Andes, prior to the collision with the Caribbean oceanic plateau. *Gondwana Research*, *66*, 207-226. https://doi.org/10.1016/j.gr.2018.10.008

Zheng, Q.; Zhang, Y.; Liu, T.; Huang, J.; Xue, N.; Shi, Q. (2017). Optimal location of vanadium in muscovite and its geometrical and electronic properties by DFT calculation. *Minerals*, *7*(3), 32. https://doi.org/10.3390/min7030032

Received: 07 january 2023
Accepted: 27 july 2023